Drug Design, Development and Therapy

Dovepress
Taylor & Francis Group

Open Access Full Text Article

ORIGINAL RESEARCH

Co-Delivery of Dacarbazine and miRNA 34a Combinations to Synergistically Improve Malignant Melanoma Treatments

Baoyue Ding[1,2,*], Mingjuan Li[2,*], Jie Zhang[2,*], Xiaojuan Zhang[2], Huan Gao[2], Jianqing Gao[3], Chunyan Shen[4], Yan Zhou[4], Fanzhu Li[5], Ailin Liu[1]

[1]Department of Pharmaceutical Analysis, Higher Educational Key Laboratory for Nano Biomedical Technology of Fujian Province, The School of Pharmacy, Fujian Medical University, Fuzhou, 350122, People's Republic of China; [2]Jiaxing Key Laboratory for Photonanomedicine and Experimental Therapeutics, Department of Pharmaceutics, Jiaxing University College of Medicine, Jiaxing, Zhejiang, People's Republic of China; [3]Institute of Pharmaceutics, Zhejiang Province Key Laboratory of Anti-Cancer Drug Research, College of Pharmaceutical Sciences, Zhejiang University, Hangzhou, Zhejiang, 310058 People's Republic of China; [4]Jiaxing Institute for Food, Drug and Product Quality Control, Jiaxing, Zhejiang, People's Republic of China; [5]Zhejiang Chinese Medical University, School of Pharmaceutical Science, Hangzhou, 310053, People's Republic of China

*These authors contributed equally to this work

Correspondence: Fanzhu Li; Ailin Liu, Email lifanzhu@zcmu.edu.cn; ailinliu@mail.fjmu.edu.cn

Purpose: The incidence of malignant melanoma (MM) has risen over the past three decades, and despite advancements in treatment, there is still a need to improve treatment modalities. This study developed a promising strategy for tumor-targeted co-delivery of Dacarbazine (DTIC) and miRNA 34a-loaded PHRD micelles (Co-PHRD) for combination treatment of MM.

Methods: To construct the dual drug-loaded delivery system Co-PHRD, poly (L-arginine)-poly (L-histidine)-polylactic acid (PLA) was employed as a building block. In this system, poly (L-arginine) and PLA function as hydrophilic and hydrophobic blocks, respectively, which self-assemble into micelles in aqueous solution. Poly(L-arginine) and poly(L-histidine) are efficiently taken up by cells and perform efficient gene condensation, which facilitate the release of encapsulated miRNA 34a into the cytoplasm. Due to its lipophilic properties, PLA can effectively encapsulate DTIC. The polypeptide aptamer DR5-TAT (D21) was used as a targeting ligand. The properties of Co-PHRD and its in vitro release behaviour were characterized. Additionally, the synergetic effects of DTIC and miRNA 34a in melanoma therapy were investigated in vitro and in vivo.

Results: Compared to DTIC treatment alone, Co-PHRD treatment exhibited 1.84-fold greater cytotoxicity in A375 cells, demonstrating that miRNA 34a enhanced the efficacy of DTIC. The particle size of Co-PHRD at an N/P ratio of 10 was 164.1 ± 4.5 nm, and the zeta potential of Co-PHRD was 27.3 ± 1.38 mV. The flow cytometry and CLSM results revealed both DTIC and miRNA 34a were avidly taken up by A375 cells at 1 h and 4 h in PHRD. In addition, in vivo results indicated that Co-PHRD micelles can significantly inhibit tumor growth without causing significant damage to major organs.

Conclusion: Co-delivery of DTIC and miRNA 34a via polypeptide micelles showed synergistic effects against MM, offering a new strategy for gene and chemotherapy.

Keywords: nano micelle, DTIC, miRNA 34a, co-delivery, malignant melanoma

Introduction

At present, the incidence of most solid tumors is decreasing or remaining the same, but the incidence of MM continues to increase.[1] There is no effective treatment for MM (the 5-year survival rate is <15%, and the mean median survival time is only 6 months).[2] Surgical resection is the primary therapeutic option for melanoma; however, surgical resection is rarely curative for patients with metastatic MM and a combination of other cancer therapeutic approaches is commonly needed. Chemotherapy, targeted therapy, and immunotherapy have been exploited clinically to treat melanoma and prolong patient survival.[3–7] DTIC, an alkylating agent, is the only US FDA-approved chemotherapeutic drug for the treatment of

Received: 21 October 2024
Accepted: 14 January 2025
Published: 24 January 2025

melanoma.[8] It functions by adding an alkyl group to the DNA of cancer cells, thereby inducing cell death.[9] However, the clinical application of DTIC in melanoma therapy is limited by several drawbacks. First, it is administered intravenously, a route that is often painful and may lead to patient noncompliance.[9] Additionally, DTIC has poor water solubility, leading to incomplete, slow, and inconsistent absorption.[10] Furthermore, DTIC is light-sensitive and unstable, contributing to its challenges in clinical use. It also causes myelosuppression, and its short half-life limits its use in combination therapies. A promising strategy to overcome these limitations is the targeted delivery of DTIC via nanocarriers, which can enhance drug delivery to melanoma cells.

Gene therapy is an alternative therapeutic option that can enhance the efficacy of melanoma therapeutics currently available, resulting in improved patient prognosis. The development of MM is related to mutations in multiple oncogenes and tumor suppressor genes. Targeting these mutant genes through gene therapy is an effective method for treating MM. RNA interference (RNAi)- and microRNA (miRNA)-based techniques represent powerful new strategies for cancer therapy.[11,12] miRNAs are single-stranded RNAs approximately 18–24 nucleotides in sizes and are chosen from an RNA duplex with an asymmetrical configuration.[13] An RNA-induced silencing complex can be formed when miRNAs cooperate with a member of the Argonaute family of proteins and other ancillary proteins. This complex can modulate the expression of target transcripts that contain corresponding cis-regulatory elements.[14] The involvement of miRNAs in determining and/or repressing the tumor phenotype, as well as its role in disease prognosis and treatment response, has been well characterized.[15,16] MiRNA 34a, a tumor suppressor that has been widely studied in recent years,[17,18] can participate in the p53 pathway and positively regulate p53 activity through inhibiting SIRTI, E2F3 and ZEB1; through this activity, miRNA 34a effectively inhibits the proliferation, invasion and metastasis of MM cells.[19,20] MiRNA 34a expression was found to be lower in metastatic melanoma cell lines compared to in situ melanoma cell lines. Overexpression of miRNA 34a significantly suppressed WM451 cell proliferation and metastasis, while miRNA 34a inhibition promoted the proliferation and metastasis of WM35 cells.[21] This was further validated in malignant melanoma harboring the wild-type p53 gene.[22] Xu et al also discovered that ZEB1 is a target of miRNA 34a in melanoma cells.[20] However, efficiently delivering miRNA to tumor cells has been a challenge. Naked miRNA molecules encounter several biological barriers, such as intravascular degradation; in addition, the molecules have short half-lives and are quickly removed.[23] The presence of a suitable delivery system is essential for overcoming these challenges.

Death receptor 4 (DR4) and Death receptor 5 (DR5) of the tumor necrosis factor-α-related apoptosis-inducing ligand (TRAIL) are highly expressed in most tumor cells, making them prime targets for active targeting therapies.[24] A synthetic peptide (YCKVILTHRCY) specifically binds to DR5,[25,26] while cell-penetrating peptides (CPPs), such as the TAT sequence (RKKRRQRRR), enhance the delivery of macromolecules across cell membranes and into the nucleus.[27,28] To combine their benefits, a multifunctional peptide (DR5-TAT) was developed by linking the DR5-targeting peptide to TAT. This peptide is designed to target DR5-expressing tumor cells, improve transmembrane delivery, and enhance gene transfection efficiency. In our previous study, we constructed a non-viral vector (Pluronic-Polyethylenimine (PEI)-DR5-TAT), which exhibited lower cytotoxicity in normal cells and higher gene transfection efficiency in tumor cells compared to PEI 25 kDa and Pluronic-PEI.[29]

Polymeric micelles have proven to be powerful vehicles for loading and delivering hydrophobic drugs, which can encapsulate hydrophobic drugs within their hydrophobic core, significantly increasing the drug's solubility in aqueous environments. This solubilization enhances the drug's ability to be absorbed in biological systems.[30] In the present study, a promising strategy for tumor-targeted co-delivery of DTIC and miRNA 34a-loaded PHRD micelles (Co-PHRD) was developed for combination treatment of MM (Figure 1). Poly(L-arginine)-poly(L-histidine)-polylactic acid (PLA) was chosen as the building block. Poly(L-arginine) and poly(L-histidine) are efficiently taken up by cells and perform efficient gene condensation, which facilitate the release of encapsulated miRNA 34a into the cytoplasm.[31] Due to its lipophilic properties, PLA can effectively encapsulate DTIC. Poly(L-arginine) and PLA serve as hydrophilic and hydrophobic blocks, respectively, which can self-assemble into micelles in aqueous solution.[32,33] To determine the targeting effect of DTIC and miRNA codelivery micelles on MM cells, we used the polypeptide aptamer DR5-TAT as a targeting ligand, which was developed in our previous research and performs tumor-targeting and pro-permeability functions.[29] The properties of Co-PHRD and its in vitro release behaviour were characterized. Additionally, the synergetic effects of DTIC and miRNA 34a in melanoma therapy were investigated in vitro and in vivo.

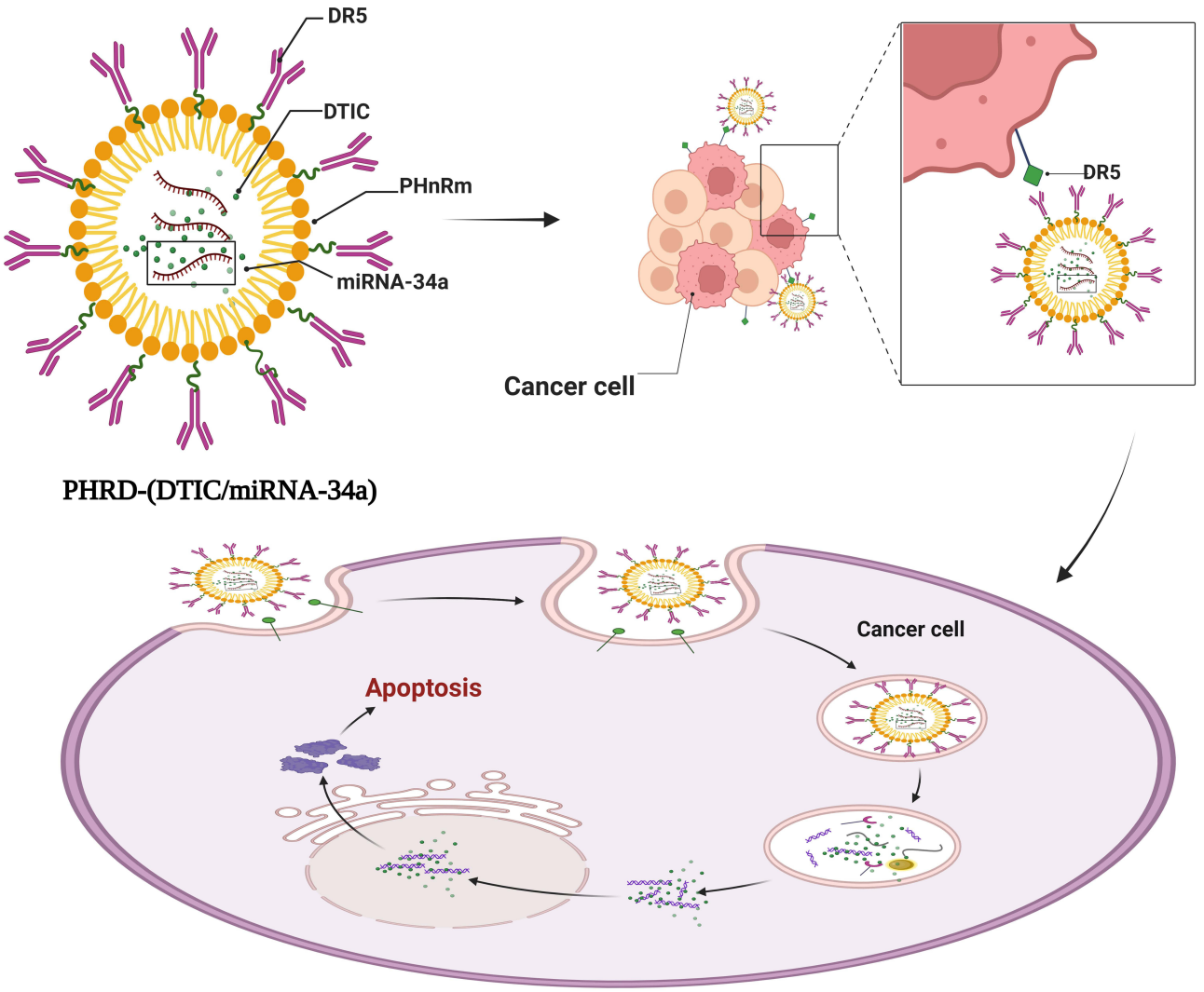

Figure 1 Schematic showing the mechanism underlying the tumor-targeted delivery of DTIC and miRNA 34a-loaded PHRD micelles (Co-PHRD).

Materials and Methods

Materials

PLA was obtained from Daigang Biological Engineering (Jinan, China). Fmoc-Arg (Pbf)-OH, Fmoc-His (Trt)-OH, and DTIC were obtained from Sigma–Aldrich (St. Louis, MO, USA). Dialysis membranes with a molecular weight cut-off (MWCO) of 500 kDa were obtained from Viskase Companies (Chicago, IL, USA). High performance liquid chromatography (HPLC)-grade methanol was obtained from OKA Chemical Reagent (Shanghai, China). MTT (3-(4,5-dimethylthiazol-2-yl)-2,5-diphenyltetrazolium bromide) was obtained from HXBIO (Hangzhou, China). Dulbecco's modified Eagle's medium (DMEM) was purchased from Gibco (Waltham, MA, USA). An RNA extraction kit was purchased from Aidlab Biotech (Beijing, China). The iScript cDNA synthesis kit and SYBR master mix were purchased from Bio-Rad (Hercules, CA, USA). A bicinchoninic acid (BCA) assay kit was acquired from Pierce (Rockford, IL, USA).

Cell Culture

Human malignant melanoma (A375) cells and mouse fibroblast (NIH-3T3) cells were purchased from the American Type Culture Collection (ATCC, Manassas, VA, USA). Cells were grown under standard culture conditions (humidified

https://doi.org/10.2147/DDDT.S497888

atmosphere composed of 95% air and 5% CO_2, 37 °C) in DMEM supplemented with 10% foetal bovine serum (FBS, Sigma–Aldrich St. Louis, MO, USA).

Synthesis and Characterization of Polymers

First, PLA was protected from hydroxy groups with tert-butyldimethylsilyl (TBDMS) and then activated with dicyclohexylcarbodiimide (DCC) and 1-Hydroxybenzotriazole (HOBt), and dicyclohexylurea (DCU) was removed by filtration. Then, H-His (Trt)-OH was added for the reaction, and TBDMS-polylactic acid-His (Trt)-OH was obtained after an overnight reaction. Next, F-moc-solid phase peptide synthesis (SPPS) was used to synthesize a histidine-arginine peptide (PH_3R_8, PHR) (Figure S1A). Second, DR5-TAT was synthesized using the same synthesis method. The products were purified by reverse HPLC. Subsequently, DR5-TAT was conjugated to PHR with N-(3-Dimethylaminopropyl)-N'-ethylcarbodiimide hydrochloride (EDC) as the coupling agent. After preparation, the product was lyophilized. The synthesized polymers were characterized by Fourier Transform Infrared Spectroscopy (FTIR) (Invitrogen | Life Technologies, Carlsbad, CA, USA) and ^{1}H-NMR at 600 MHz (Varian, Palo Alto, CA, USA) in deuterium oxide (Figure S1B).

Preparation and Characterization of Co-PHRD Nanomicelles

In this study, drug-loaded micelles were prepared by ultrasonic emulsification. Briefly, 1 mg of DTIC was dissolved in methanol at a concentration of 1 mg/mL. PHRD was dissolved in doubly distilled water to a concentration of 1 mg/mL. The DTIC solution was slowly added to the PHRD solution and sonicated twice in an ice bath for 30s at 100 W. Next, the mixture was directly transferred to 5 mL of doubly distilled water and magnetically stirred in a fume hood overnight at room temperature (RT) to evaporate the methanol. The micelle suspension was centrifuged at 10,000 rpm for 15 min. The supernatant was then passed through a 0.45-μm syringe filter to eliminate any residual polymer or DTIC aggregates. The Co-PHRD was prepared by mixing the miRNA 34a plasmid with different N/P ratios (the ratio between the nitrogen of amine in polymers to that of the phosphate in DNA) of PHRD/DTIC, and the mixture was incubated at RT for 30 min to electrostatically bind the negative miRNA 34a plasmid to the positive surface of the nanomicelle. All procedures were carried out in the dark.

Characterization of Micelles Size and Zeta Potential of the Complex

Freeze-dried nanomicelles were dispersed in deionized water (pH 7.0). The average size and zeta potential of the Co-PHRD were analysed using a dynamic light-scattering detector (Litesizer 500, Anton Paar, Austria). At least three different batches were analysed to determine the average value and standard deviation for the particle diameter and zeta potential. The morphology of Co-PHRD was observed using transmission electron microscopy. Briefly, after the Co-PHRD was lyophilized, the dried nanoparticles were resuspended in deionized water. The samples were prepared by placing one drop of a dilute dispersion onto a copper grid coated with a carbon membrane. The surface morphology of the Co-PHRD samples was then visualized by transmission electron microscopy (TEM) (H600, Hitachi, Tokyo, Japan).

Measurement of the Critical Micelle Concentration (CMC) of PHRD

The micellization behaviours of PHRD were confirmed by measuring the CMC by utilizing a pyrene fluorescence probe.[34] Briefly, a 6×10^{-6} M hydrazine solution was prepared with acetone as the solvent, the acetone was naturally volatilized, and a blank micelle solution was added to a volumetric flask containing a small amount of bismuth. Then, the volume was adjusted to a series of concentrations from 5.0×10^{-5} to 2.0 mg/mL (1×10^{-5}, 5×10^{-5}, 1×10^{-4}, 5×10^{-4}, 1×10^{-3}, 5×10^{-3}, 0.01, 0.05, 0.1, 0.5, 1, 2). After incubation for 2 h or more at 25 °C in the dark, the fluorescence spectra of each solution were measured in a fluorescence spectrophotometer (Hitachi F-7000, Japan). The excitation wavelength of the fluorescence scan was 333 nm, the excitation wavelength was set to 5.0 nm, the emission wavelength was set to 2.5 nm, and the scanning speed was 500 nm/min. Fluorescence values at wavelengths of 373 nm (I_1) and 383 nm (I_3) were recorded, with the logarithm of the blank vector concentration as the abscissa and I_1/I_3 plotted on the ordinate.

Agarose Gel Electrophoresis

The ability of the micelles to condense miRNA 34a was determined by agarose gel electrophoresis. miRNA 34a was diluted with diethyl pyrocarbonate (DEPC) water and blank-PHRD or PHRD/DTIC. PHRD/DTIC was diluted with double-distilled water. An appropriate amount of miRNA 34a was then added to the solution containing Blank-PHRD or PHRD/DTIC to generate PHRD/miRNA 34a and Co-PHRD, respectively, at an N/P ratio of 0.5–40. The complexes were incubated for 30 min at RT. PBS buffer solution containing dithiothreitol (DTT; 10 μL) was added to above solution to give a final concentration of 10 mm DTT, and were incubated for 1 h. The samples were then electrophoresed at 100 V for 20 min on a 1.0% (w/v) agarose gel with GelRed stain in Tris-acetate-EDTA (TAE) buffer. The gel was subsequently photographed using a UV illuminator.

The Co-PHRD and PHRD/ miRNA 34a were mixed with different concentrations of heparin sodium and incubated at 37°C for 2 h to displace miRNA. PEI 25K/miRNA 34a polyplexes were the control group. The samples were then assessed by agarose gel electrophoresis and photographed using a UV illuminator as described above.

Evaluation of Drug Contents

The concentration of DTIC was determined by HPLC. The mobile phase was methanol: water (30/70, v/v); the flow rate was 1.0 mL/min; the UV detection wavelength was 319 nm; and the column was a C18 column (Diamonsil, 5 μm, 250×4.6 mm). The column temperature was 30 °C, and the drug loading rate (DL) and encapsulation efficiency (EE) were calculated as follows:

DL (%) = (weight of loaded drug/total weight of polymer and loaded drug) ×100%.

EE (%) = (weight of loaded drug/weight of drug in feed) × 100%.

In vitro Release Study

A dialysis membrane with a cut-off of 500 Da (MWCO) was selected to investigate the in vitro release of the Co-PHRD drug-loaded micelles. For that purpose, 2 mL of the Co-PHRD aliquot suspension was diluted with phosphate-buffered saline (PBS) (pH 7.4, final volume 50 mL) in a capped beaker. The beakers were incubated at 37°C and shaken horizontally at 120 strokes/minute. The specified time periods were 1, 2, 4, 6, 8, 10, 12, 24, 48, and 72 h. The amount of residual DTIC in the nanomicelles was determined by HPLC using the same procedure as described above. The amount of released drug was quantified, and the cumulative release profile over time was determined. The amount of drug released over time was expressed as a percentage of the initial drug load in the nanoparticles. All tests were performed in triplicate.

Cellular Uptake and Intracellular Distribution

To investigate the cellular uptake of chemotherapeutic drugs mediated by the PHRD carrier, A375 cells were seeded at a density of 3×10^5 cells/well in a 12-well plate with 6 replicates per group. Each well was supplemented with serum-free DMEM to a final volume of 1 mL, and the plates were incubated in a CO_2 incubator for 24 h. After removing the old medium, Fluorescein (FAM)-labeled miRNA 34a was added. Freshly prepared PHRD- phycoerythrin (PE) (prepared similarly to PHRD-DTIC), PHRD-FAM-miRNA 34a, PHRD-DTIC-FAM-miRNA 34a, and PHRD-PE-miRNA 34a were then introduced, and the plates were incubated for an additional 1 h and 4 h. The medium was then discarded, and the cells were washed once with PBS, digested with trypsin, and centrifuged at 400 g for 5 min to collect the cells. The cell pellet was washed once in PBS and resuspended in 300 μL of PBS. Untreated cells served as a negative control. Flow cytometry was used to analyze the uptake of PE-phycoerythrin and FAM-miRNA 34a by A375 cells.

The intracellular distribution of DTIC and miRNA 34a was examined using confocal laser scanning microscopy (CLSM). A375 cells were seeded at a density of 5×10^4 cells/well in a 12-well plate containing glass coverslips and allowed to grow for 24 h. Free PE, PHRD/PE, PHRD/FAM-miRNA 34a, and PHRD/(PE/FAM-miRNA 34a) (100 nM FAM-miRNA 34a, N/P ratio of 10:1) were then added to the cells with 6 replicates per group. After 1 h and 4 h of incubation, the medium was removed, and the cells were washed twice with PBS. The cells were fixed with 4% paraformaldehyde (v/v) and the nuclei were stained with 4',6-diamidino-2-phenylindole (DAPI). The cells were then mounted with sealing medium and visualized using a confocal laser scanning microscope (Nikon, Japan).

MTT Assay for the Cytotoxicity of the Cells

Cell viability was assessed by MTT assay. Briefly, cells ($1x10^4$) were seeded in 96-well plates and incubated in DMEM supplemented with 10% FBS until the cells reached 60% confluence. The cells were then treated with Blank-PHRD, DTIC, miRNA 34a plasmid, PHRD/DTIC, PHRD/miRNA 34a and Co-PHRD for 72 h with 6 replicates per group. Blank control wells received fully supplemented DMEM medium. MTT solution at 5 mg/mL was added, and the mixture was incubated for an additional 4 h. After incubation, the supernatants were removed, and the remaining water-insoluble formazan crystals were dissolved in 150 μL of DMSO for 10 min with gentle shaking. The optical density was measured at 490 nm using a multiwell plate reader (Invitrogen Life Technologies, Carlsbad, CA, USA). The percentage of viable cells was calculated and compared with that of the control cells.

Determination of the Combination Index Value

To evaluate the combination effect of DTIC and miRNA 34a, PHRD/DTIC and PHRD/miRNA 34a, preincubated A375 cells were cotreated with various concentrations of drug and drug-loaded PHRD for 72 h with 6 replicates per group. Cell viability was determined by the same MTT assay method described above and analysed by CompuSyn software, which follows the median effect principle, to determine the combination index (CI) value. A combination index (CI) value <1, =1 or >1 indicates synergism, an additive effect or antagonism, respectively.

Flow Cytometric Analysis of Apoptosis

Apoptosis was measured by flow cytometry as described previously. Briefly, A375 cells were seeded at 2×10^5 cells per well in 6-well plates and treated with DTIC, miRNA 34a, DTIC +miRNA 34a, PHRD/DTIC, PHRD/miRNA 34a, or Co-PHRD loaded with the same amount of DTIC and miRNA 34a for 72 h with 6 replicates per group. The cells were then collected and stained with Annexin V-FITC/PI at room temperature in the dark, and apoptosis was measured by flow cytometry (BD Biosciences, San Jose, CA, USA). The percentages of Annexin V+/PI- (early apoptotic) and Annexin V +/PI+ (late apoptotic) cells were calculated according to the manufacturer's instructions (BD, USA).

In Vivo Evaluation of Antitumor Effect and Safety

All the experimental procedures were conducted following the Guide for the Use and Care of Laboratory Animals of the National Institutes of Health. A total of 48 male BALB/c nude mice (4 wk old) were housed in a specific pathogen-free (SPF) environment. After 2 weeks of adaptation, the mice were randomly divided by weight into 6 groups. A375 cells were injected subcutaneously (s.c). into the left flank of each nude mouse (5×10^6 cells in 200 μL of PBS) (D0). A375 tumor-bearing BALB/c nude mice with a tumor size of approximately 100 mm^3 (D14) in the left flank were randomly divided into the following groups (n=6): (1) the normal saline control group, (2) the blank PHRD group, (3) the free DTIC group, (4) the PHRD/DTIC group, (5) the PHRD/miRNA 34a group, and (6) the Co-PHRD group (DTIC equivalent of 10 mg/kg and miRNA 34a of 2 mg/kg). A total of 12 mice were screened out as the tumor volumes deviated 100 mm^3 too much (from 8 mm^3 to 15 mm^3). The drugs were injected through the tail vein every 4 days from D14. Tumor volumes and body weights were measured every other day, and palpable tumors were measured in two dimensions (length and width) using a digital Vernier calliper (0.01 mm). Tumor volume was calculated using the following equation: V (mm^3) = (length × $width^2$)/2. The tumor inhibitory rate (TIR) was calculated using the following equation: $TIR = [1 - (W_{test} - W_{initial})/(W_{saline} - W_{initial})] \times 100\%$, where W_{test} is the final mean tumor weight of the tested groups, $W_{initial}$ is the initial mean tumor weight of the tested groups, and W_{saline} refers to the final mean tumor weight of the saline group. The lived mice were euthanized properly on D32. The tissues of the tumor, heart, liver, spleen, lung, and kidney were collected and stored in 4% paraformaldehyde overnight, which were then stained with hematoxylin and eosin (H&E).

Statistical Analysis

GraphPad Prism 9 (GraphPad Software, La Jolla, CA, USA) was used for all the statistical analyses. The data are expressed as the means ± SD. Differences between groups were examined for statistical significance by t tests. Two-sided P values were calculated, and a value of $P<0.05$ was considered to indicate statistical significance.

Results and Discussions

Particle Size, Zeta Potential, Morphology and CMC of Co-PHRD Micelles

Co-PHRDs with different N/P ratios were prepared, and their mean diameters and zeta potentials were measured. As shown in Figure 2A and B, all the micelles had a positive surface charge with a zeta potential range, and the particle sizes of all the micelles with different N/P ratios were less than 200 nm, except for those with an N/P ratio of 40. The particle size of Co-PHRD at an N/P ratio of 10 was 164.1 ± 4.5 nm (Figure 2C), and the polydispersity index (PDI) was 0.269 ± 0.780. Due to the reasonable size of Co-PHRD, it was suitable for systematic administration through the enhanced permeability and retention (EPR) effect of the delivery system.[35] The zeta potential of Co-PHRD was 27.3 ± 1.38 mV (Figure 2D), which was conducive to strong electrostatic interactions between the complexes and cell membranes for increased uptake efficiency. In further, positively charged constructs, such as cationic liposomes and polymers, are essential for nonviral gene transfection. They interact with cell membranes, facilitating endocytosis, while mechanisms like the "proton sponge" effect prevent DNA degradation in lysosomes, enabling DNA release into the nucleus for integration.[36] The morphological characteristics of the Co-PHRD were assessed using TEM. As shown in Figure 2C, they had a spherical and compact nanostructure. As indicated by the sigmoidal curve presented in Figure 2E, the micellization behaviours of PHRD were confirmed by measuring the CMC by utilizing a pyrene fluorescence probe. The

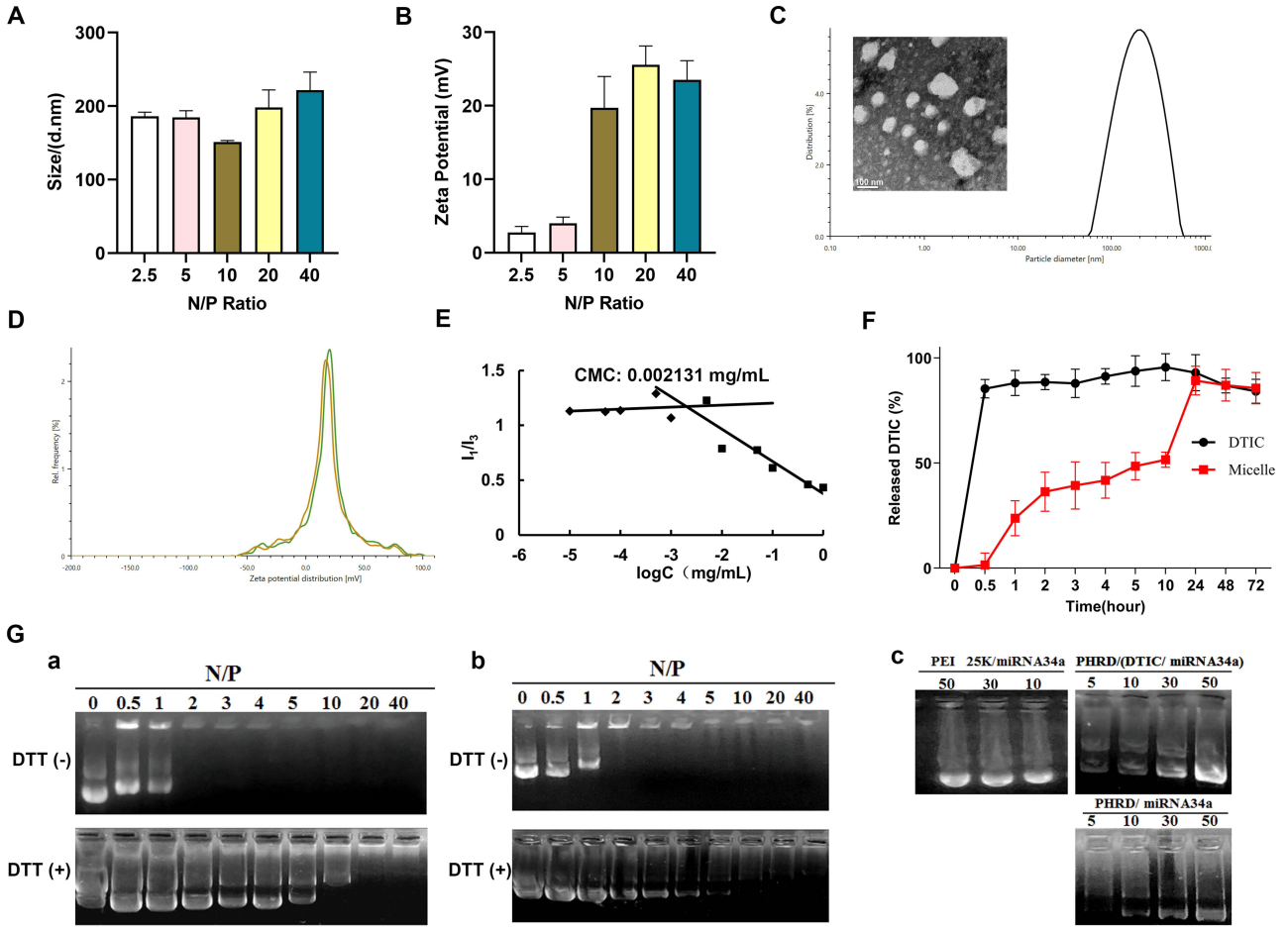

Figure 2 Characterization of Co-PHRD micelles. (**A**) Particle size of Co-PHRD determined by DLS. Size-related values represent mean ± SD of 3 repeated measurements. (**B**) Zeta potential of Co-PHRD determined by DLS, values were represented as mean ± SD from 3 repeated measurements. (**C**) Particle size and TEM images of PHRD/(DTIC/miRNA 34a) at an N/P ratio of 10 determined by DLS (scale bar = 100 nm). (**D**) Zeta potential of Co-PHRD at an N/P ratio of 10 determined by DLS. (**E**) CMC of Co-PHRD micelles determined using fluorescence spectra of the pyrene probe at different concentrations of PHRD (1×10^{-5} - 2.0 mg/mL). (**F**) Profiles of DTIC release from Co-PHRD. Values were represented as mean ± SD from 3 repeated measurements. (**G**) Agarose gel electrophoresis results: a) miRNA 34a binding affinity for PHRD at various N/P ratios in the presence or absence of DTT, b) miRNA 34a binding affinity for PHRD/DTIC at various N/P ratios in the presence or absence of DTT and c) heparin competition assay with different amounts of heparin sodium with PEI 25K/miRNA 34a, PHRD/miRNA 34a and Co-PHRD. The data are expressed as the means ± SDs (n= 3).

https://doi.org/10.2147/DDDT.S497888

intensity ratio of I_1/I_3 was low at a relatively low polymer concentration, revealing the characteristics of pyrene present in aqueous environments. However, the intensity increased dramatically when the polymer concentration was increased to that of CMC, indicating that pyrene was present in the hydrophobic environment of the formed polymeric micelles (Figure 2C). The CMC of Co-PHRD was as low as 0.002131 mg/mL, suggesting that the PHRD micelles are stable within the body following intravenous injection. The drug loading rate (DL) and encapsulation efficiency (EE) were 29.25 ± 3.23 μg/mg and 78.3 ± 5.71%, respectively.

Release Behaviour of DTIC-Loaded Micelles in Vitro

We next evaluated the release pattern of DTIC from Co-PHRD at pH 7.4 at 37 °C using a dialysis method. As shown in Figure 2F, when DTIC is released from micelles, a sudden release effect occurs first, which may result from some drugs adhering to the hydrophilic chain segment outside the micelles; then, a slow release process occurs. After 72 h, 85.6% of the DTIC was released from the DTIC-loaded micelles. The results showed that DTIC encapsulated in micelles had a certain sustained release effect, which provided a basis for increasing the stability of drugs and prolonging their action time.

Condensation and Protection Ability of Co-PHRD Micelles

The condensation ability of the complexes was determined by agarose gel electrophoresis. A complete mobility shift of miRNA 34a was achieved at an N/P ratio of 10 (Figure 2G). To verify whether polymerization affects the binding ability to miRNA 34a, DTT (a reducing agent analogous to glutathione) was added to break the disulfide bonds.[34] The results showed that PHRD had a weaker miRNA 34a binding affinity in the presence of DTT. Based on the electrophoresis results in the presence of DTT, we hypothesized that the disulfide crosslinked peptides could dissociate in the reducing environment of the cytoplasm, which should effectively release the drug and miRNA 34a. A heparin competition assay was also performed to assess the resistance of the strains to strong polyanions. As shown by the strong band signals, control PEI 25K/miRNA were completely disrupted at an ambient heparin concentration, indicating that the encapsulating capability had been weakened. In contrast, Co-PHRD micelles strongly retained siRNA molecules even at high heparin concentrations (up to 20 μg/mL), indicating that they have superior resistance to competitively strong polyanions. Based on the stability results, it is reasonable to conclude that these complexes can be used in systems for delivering miRNA 34a in vivo.

Cellular Uptake

Effective uptake into cells is necessary for effective cancer therapy. Since DTIC is nonfluorescent, PE, a fluorescence probe, was placed into micelles as a substitute for DTIC. To investigate the cellular uptake of miRNA 34a mediated by Co-PHRD micelles, miRNA 34a was labelled with a FAM probe. After 1 and 4 h of incubation, the cellular uptake of free PE, PHRD-PE, FAM-miRNA 34a and PHRD-FAM-miRNA 34a was compared by flow cytometry (Figure 3A-D). The flow cytometry results showed that the uptake rates of DTIC and miRNA 34a were greater in PHRD compared to the control. Following flow cytometry, CLSM was performed to investigate the temporal kinetics of intracellular distribution of DTIC and miRNA 34a. As showed in Figure 3E and F, after incubation with Co-PHRD 1 and 4 h, PE and FAM-miRNA 34a (green fluorescence) were observed in the perinuclear region of the cytoplasm. The white fluorescence resulting from the overlay of red, green, and blue DAPI nuclear fluorescence in the merged image indicates that PHRD-PE and FAM-miRNA 34a were effectively codelivered by Co-PHRD micelles into A375 cells. This finding corresponds well with the flow cytometry results.

Antiproliferation Assay

The cytotoxicity of Blank-PHRD, free DTIC, PHRD-DTIC, miRNA 34a and Co-PHRD in A375 cells was subsequently monitored using a cell viability assay. As shown in Figure 4A, no significant cell toxicity was observed in A375 or NIH3T3 cells after 72 h of incubation with blank-PHRD (0.1–100 μg/mL). In contrast, cytotoxicity was observed in dose-dependent manner in the groups treated with free DTIC, PHRD-DTIC, miRNA 34a and PHRD- miRNA 34a in A375 cells (Figure 4B and C). The inhibitory effect of PHRD-DTIC was greater than that of free DTIC at almost all

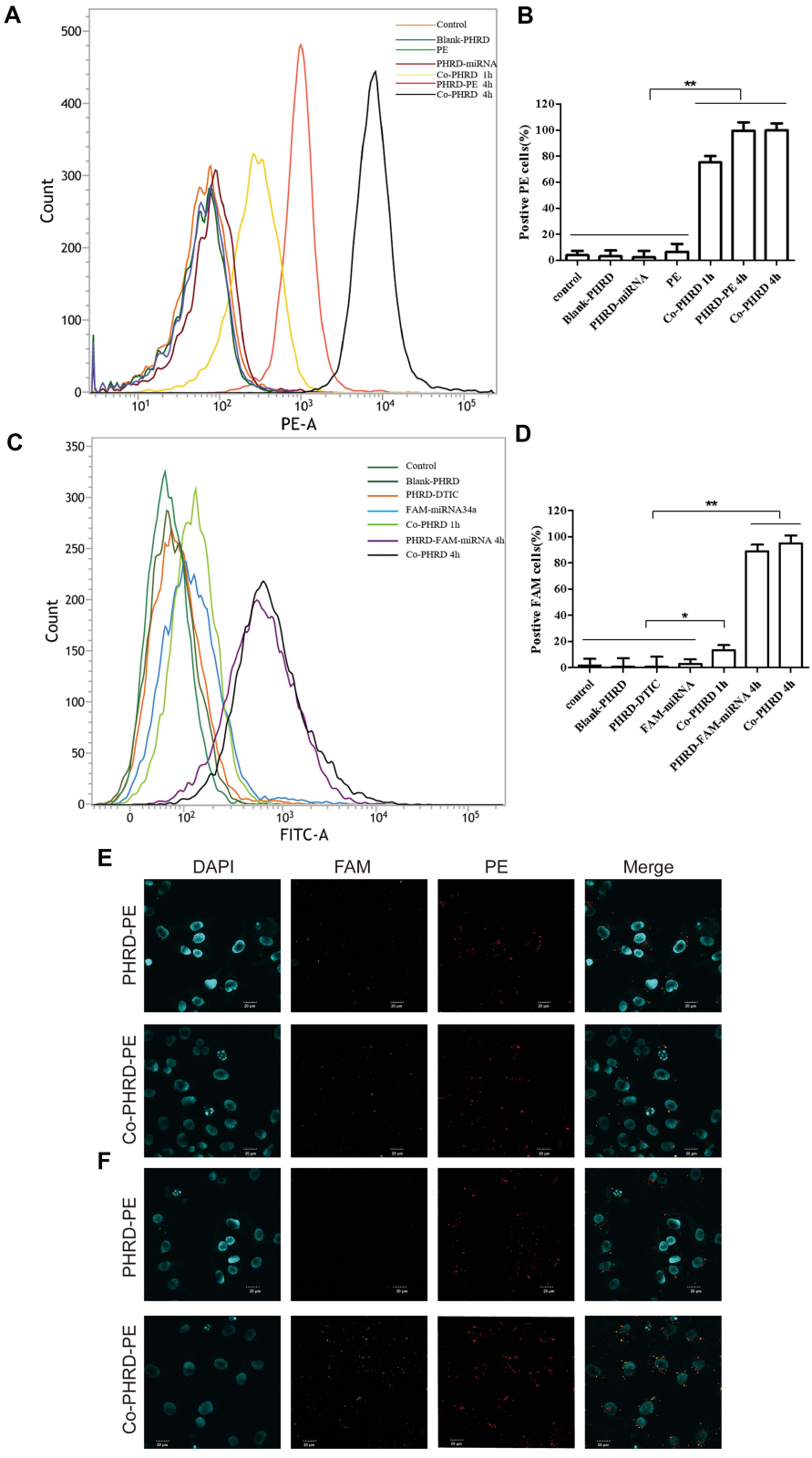

Figure 3 Cellular uptake of PE-DTIC and FAM-miRNA 34a. (**A** and **B**) Quantitative analysis of the mean fluorescence intensity of PE. The data in B are expressed as the means ± SDs (n= 6). (**C** and **D**) Quantitative analysis of the mean fluorescence intensity of FAM. The data in D are expressed as the means ± SDs (n= 6). (**E** and **F**) Confocal microscopy Images of A375 cells after 1 h (**E**) and 4 h (**F**) of incubation with PE, PHRD-PE, PHRD/FAM-miRNA 34a, or Co-PHRD, respectively (n=3). Green signals represent FAM-labelled miRNA 34a, red signals represent PE, and blue signals represent DAPI-stained cell nuclei. The scale bar is 20 μm (PHRD/FAM-miRNA 34a and Co-PHRD at N/P= 10). *p <0.05, **p <0.01.

https://doi.org/10.2147/DDDT.S497888

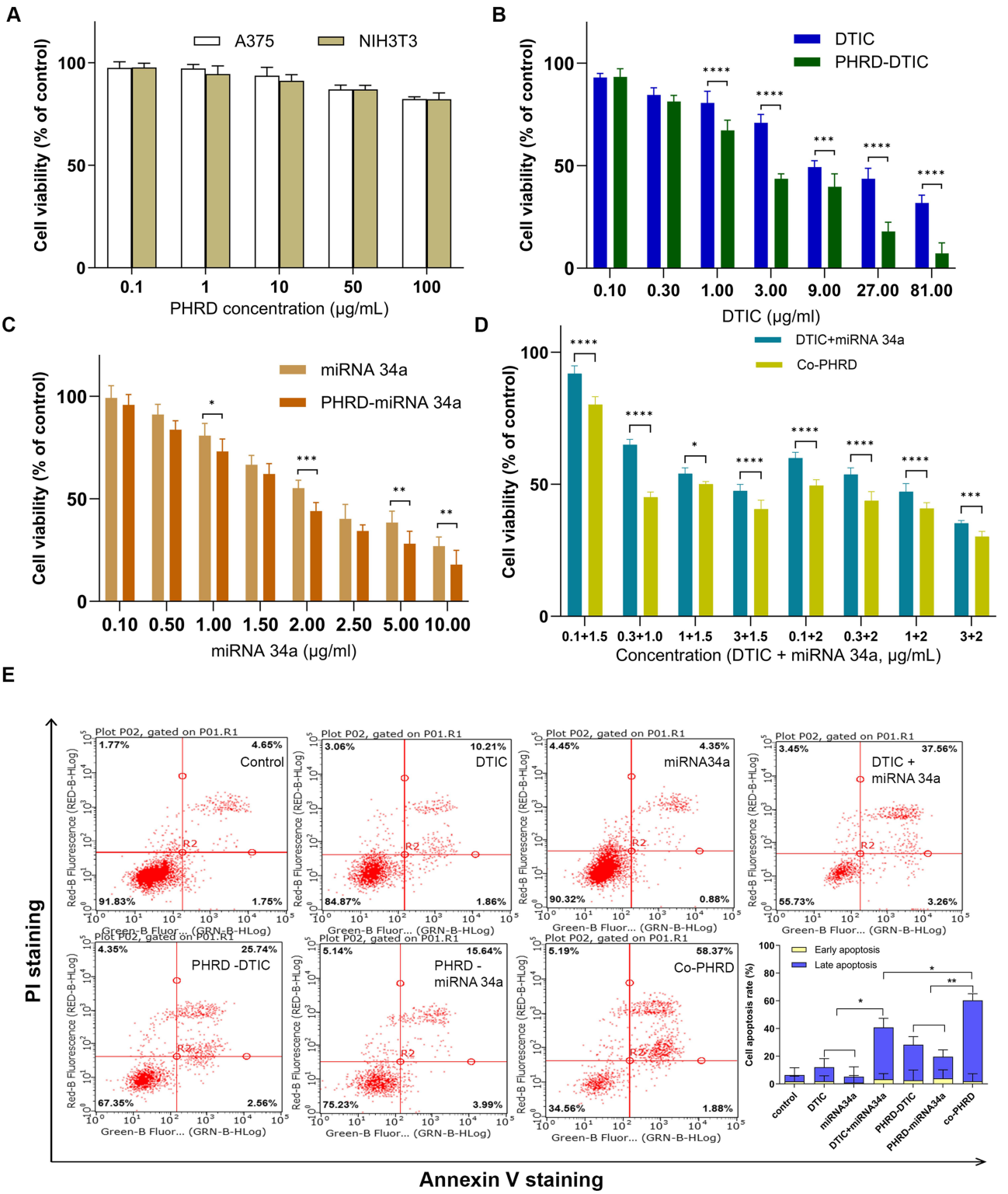

Figure 4 In vitro antitumor effect of Co-PHRD. (**A**) Viability of A375 and NIH3T3 cells treated with different concentrations of Blank-PHRD for 72 h. Dose-dependent cell viability of A375 cells treated with DTIC, PHRD-DTIC (**B**), miRNA 34a, or PHRD-miRNA 34a (**C**) and DTIC + miRNA 34a or Co-PHRD (**D**) for 72 h. MTTwas used to assess cell viability. The data in A-D are expressed as the means ± SDs (n= 6). (**E**) Apoptosis analysis of A375 cells after 72 h of treatment with different formulations, as measured by flow cytometry using an Annexin V-APC kit and PI staining. The data are expressed as the means ± SDs (n= 3). *p <0.05, **p <0.01, ***p <0.001, **** p <0.0001.

https://doi.org/10.2147/DDDT.S497888

concentrations, probably due to the rapid uptake of nanocarriers with a size of ~150 nm and the sustained release of DTIC from PHRD-DTIC. The calculated IC50 in the PHRD-DTIC and PHRD- miRNA 34a was lower than free DTIC and free miRNA 34a groups at 72 h (2.609 ± 2.425 μg/mL vs 6.287 ± 4.106 μg/mL; 1.81 ± 5.13 μg/mL vs 1.894 ± 4.627 μg/mL, respectively). We also investigated the cytotoxicity of the combined use of DTIC and miRNA 34a as well as Co-PHRD at different ratios. As shown in Figure 4D, the cytotoxicity of Co-PHRD was significantly higher compared to that of the drugs used in combination individually. In conclusion, PHRD-loaded DTIC and miRNA34a could enhance the anti-proliferative effect on A375 cells.

Cell Apoptosis Assays

The percentages of apoptotic cells in the DTIC, miRNA 34a, DTIC + miRNA 34a, PHRD-DTIC, PHRD-miRNA 34a and Co-PHRD groups were 12.07%, 5.23%, 40.82%, 28.3%, 19.63% and 60.25%, respectively (Figure 4E). The Co-PHRD group exhibited the highest level of cell apoptosis, suggesting that the simultaneous delivery of miRNA 34a and DTIC, which was mediated by PHRD micelles, increases the efficacy of DTIC, provides synergistic effects and increases the rate of cell apoptosis.

Synergistic Effect of DTIC and miRNA 34a Treatment on the A375 Cell Line

A synergistic effect on cell apoptosis mediated by DTIC and miRNA 34a was also observed in A375 cells. The combination of DTIC and miRNA 34a significantly inhibited the growth of A375 cells. As shown in Figure 5A-C, at a dose of 3 μg/mL DTIC and 1 μg/mL miRNA 34a, the minimum CI value was CI<1. Figure 5D-F shows that at a dose of 1 μg/mL PHRD-DTIC and 0.5 μg/mL PHRD-miRNA 34a, the minimum CI value was CI<1; these results suggest that the drug-loaded micelles Co-PHRD can synergistically inhibit A375 cell proliferation at low concentrations.

Antitumor Efficacy in the MM Xenograft Model

The in vivo therapeutic efficacy of Co-PHRD against A375 in a xenograft nude mouse model was further tested. The tumor volumes and weights of the mice were monitored at regular intervals (Figure 6A). Tumor growth was significantly less inhibited in the Blank-PHRD group than the PHRD-DTIC, PHRD-miRNA and Co-PHRD groups. The free DTIC, PHRD-DTIC, PHRD-miRNA 34a and Co-PHRD groups all exhibited different levels of tumor suppression (Figure 6B, D and E). Compared with the other groups, the Co-PHRD group showed significant anti-tumor activity ($P < 0.01$), suggesting that DTIC and miRNA 34a exerted synergistic effects on A375 solid tumors in vivo. This result was also confirmed by the difference in the mean weight of the tumors isolated on Day 32 (Figure 6B) ($P < 0.05$). We observed that all groups of mice generally maintained their body weight, suggesting an absence of notable systemic toxicity throughout the treatment (Figure 6C). Additionally, tissue H&E staining images showed that the administration of all therapeutic agents caused no significant damage to major organs, including the heart, liver, spleen, lungs, and kidneys (Figure 6F).

Summary

We successfully developed the Co-PHRD polypeptide micelle system for the co-delivery of miRNA-34a and DTIC. Our findings demonstrate that this system effectively inhibited melanoma cell proliferation, induced significant apoptosis, suppressed cell cycle progression and migration, and enhanced antitumor efficacy both in vitro and in vivo. Furthermore, the micelle system shows substantial potential for application in the combined treatment of human cancers. However, as this study was preliminary and conducted in melanoma cell lines, it has certain limitations. Additional modifications to the carrier system may be necessary to improve stability and delivery efficiency in more complex biological environments. Future research will focus on expanding these studies to a wider range of clinically relevant animal models to further validate the system's therapeutic potential.

Abbreviations

MM, Malignant melanoma; DTIC, Dacarbazine; miRNA, MicroRNA; siRNA, Small interfering RNA; CCK-8, Cell Counting Kit-8; EC_{50}, Median effect concentration; IC_{50}, Half-maximal inhibitory concentration; RNAi, RNA

A

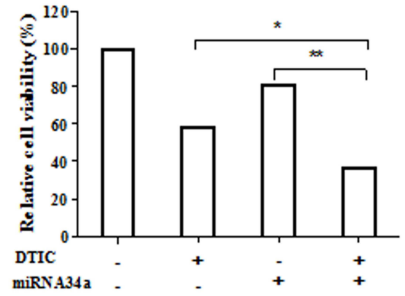

B

DTIC (μg/ml)	miRNA34a (μg/ml)	Fa	CI values
(1) 3	(1) 1	0.3689	0.32254
(2) 1	(2) 1	0.4864	0.42076
(3) 0.3	(3) 1	0.585	0.51822
(4) 3	(4) 1.5	0.4745	0.67833
(5) 3	(5) 2	0.352	0.55345
(6) 1	(6) 1.5	0.54	0.72153
(7) 0.1	(7) 1	0.6893	0.68651
(8) 1	(8) 2	0.472	0.75379
(9) 0.3	(9) 1.5	0.6503	0.93744
(10) 0.3	(10) 2	0.5371	0.86776

C

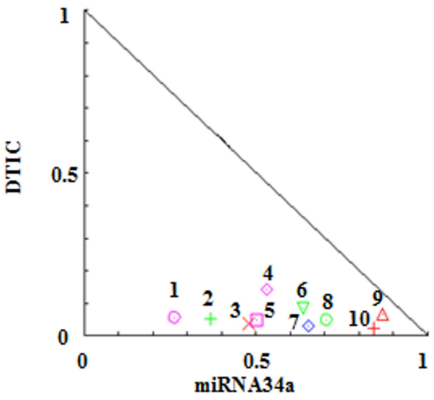

D

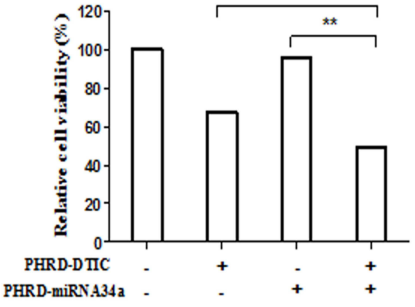

E

PHRD-DTIC (μg/ml)	PHRD-miRNA34a (μg/ml)	Fa	CI values
(1) 3	(1) 0.5	0.4005	0.70414
(2) 1	(2) 0.5	0.4927	0.54394
(3) 0.3	(3) 0.5	0.6675	0.73028
(4) 0.3	(4) 1	0.485	0.55198
(5) 0.3	(5) 1.5	0.451	0.68496
(6) 0.3	(6) 2	0.4371	0.84170

F

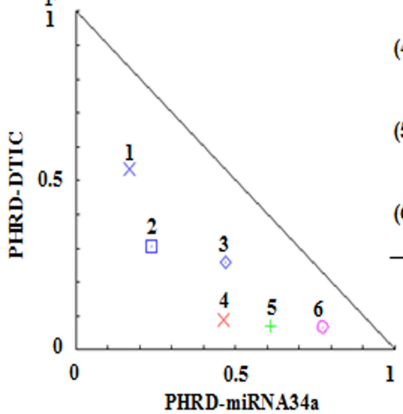

Figure 5 Combination effect of DTIC and miRNA 34a, PHRD-DTIC and PHRD-miRNA 34a. Preincubated A375 cells were cotreated with DTIC (0.1–3 μg/mL) and miRNA 34a (0.5–2 μg/mL) for 72 h (**A** and **B**) (n=6). Cell viability was determined by the MTT assay. The combination effect was analysed by CompuSyn software, which follows the median effect principle to determine the combination index (CI) value (**C**). Preincubated A375 cells were cotreated with PHRD-DTIC (0.1–3 μg/mL) and PHRD-miRNA 34a (0.5–2 μg/mL) for 72 h (**D** and **E**). The combination effect was analysed by CompuSyn software (**F**). *p <0.05, **p <0.01.

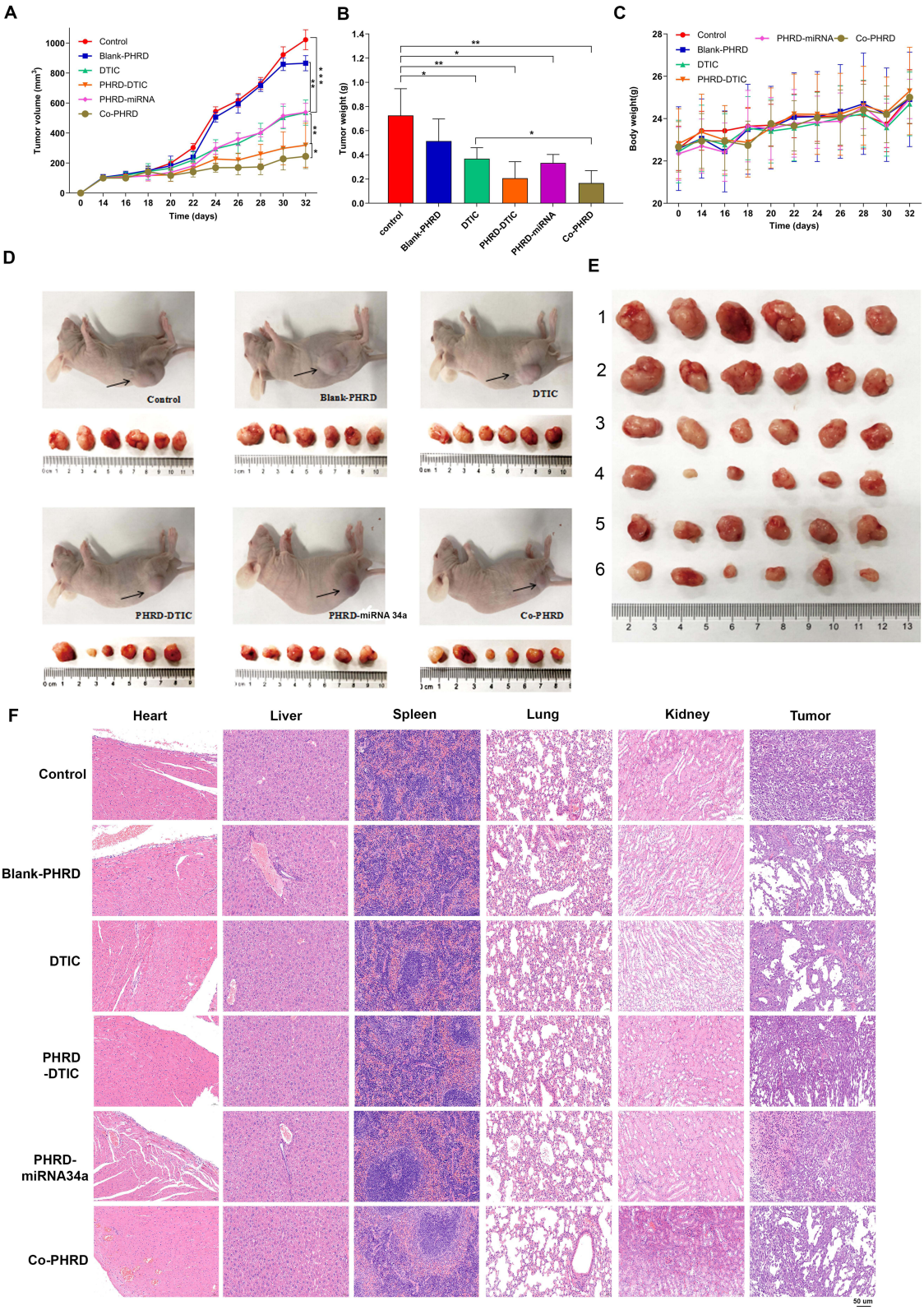

Figure 6 (**A**) Tumor growth curves of mice receiving different therapeutic regimens (n =6, mean ± SD). (**B**) Tumor weights of mice receiving different therapeutic regimens (n =6, mean ± SD). (**C**) The mouse weights did not differ between the groups that received different therapeutic regimens and the control group. (**D**) Gross appearance of mice bearing MM xenografts after 32 days of treatment with different therapeutic regimens. (**E**) All tumors that had been excised from the mice are shown, corresponding to the groups designated above in Panel D. (**F**) Results of H&E staining of different organs and tumors in nude mice. Scale bar = 50 μm. $^{**}p < 0.01$, $^{***}p < 0.001$.

https://doi.org/10.2147/DDDT.S497888

interference; DR4, Death receptor 4; DR5, Death receptor 5; TRAIL, Tumor necrosis factor-α-related apoptosis-inducing ligand; PEI, Polyethylenimine; CPPs, Cell-penetrating peptides; PLA, Poly(L-arginine)-poly(L-histidine)-polylactic acid; TME, Tumor microenvironment; CMC, Cell-mediated cytotoxicity; CI, Combination index; PDI, Polydispersity index; OS, Overall survival; PD-1, Programmed death 1; MHC, Major histocompatibility complex; SPF, Specific pathogen-free; FBS, Foetal bovine serum; ATCC, American Type Culture Collection; A375, Human malignant melanoma cells; NIH-3T3, Mouse fibroblast cells; TBDMS, Tert-butyldimethylsilyl; DCC, Dicyclohexylcarbodiimide; DCU, Dicyclohexylurea; HOBt, 1-Hydroxybenzotriazole; SPPS, Solid phase peptide synthesis; HPLC, High Performance Liquid Chromatography; EDC, N-(3-Dimethylaminopropyl)-N'-ethylcarbodiimide hydrochloride; FTIR, Fourier Transform Infrared Spectroscopy; DEPC, Diethyl pyrocarbonate; DTT, Dithiothreitol; DL, Drug loading; EE, Encapsulation efficiency; FAM, Fluorescein; RT, Room temperature; TAE, Tris-acetate-EDTA buffer; s.c., Subcutaneously; CLSM, Confocal laser scanning microscopy; DAPI, 4',6-diamidino-2-phenylindole; ERP, Enhanced permeability and retention; TNF-α, Tumor necrosis factor-α; LPS, Lipopolysaccharide; FITC, Fluorescein isothiocyanate; PE, Phycoerythrin; H&E, Hematoxylin-eosin; APC, Allophycocyanin; PBS, Phosphate-buffered saline; TGI, Tumor growth inhibition value; TEM, transmission electron microscopy.

Data Sharing Statement

All data associated with this study are present in the paper and the Supplementary Materials.

Ethics Approval and Informed Consent

The animal research involved in this study was approved by the Laboratory Animal Ethics Committee of College of Medicine, Jiaxing University (Ethical No. JUMC2021-138) and performed in accordance with the Guideline for Ethical Review of Animal Welfare (No. GB/T 35892-2018).

Consent for Publication

All named authors agreed to submit the manuscript for publication.

Author Contributions

All authors made a significant contribution to the work reported, whether that is in the conception, study design, execution, acquisition of data, analysis and interpretation, or in all these areas; took part in drafting, revising or critically reviewing the article; gave final approval of the version to be published; have agreed on the journal to which the article has been submitted; and agree to be accountable for all aspects of the work.

Funding

This work was supported by the National Natural Science Foundation of China (81872220 and 81703437), Basic Public Welfare Research Project of Zhejiang Province (LGF18H160034, LGD20H300001, LTGY24H160007 and LGD21H300001), Key Research and Development and Transformation project of Qinghai Province (2021-SF-C20), Science and Technology Bureau of Jiaxing (2024AY10009 and 2024AY10042), National College Students' Innovation and Entrepreneurship Training Program (202110354017), Tumor Nanotargeting and TCM Technology Innovation Team (Key Science and Technology Innovation Team of Jiaxing, 2018), and Jiaxing Key Laboratory of Oncological Photodynamic Therapy and Targeted Drug Research.

Disclosure

The authors declare that they have no conflicts of interest for this work.

References

1. Siegel RL, Giaquinto AN, Jemal A. Cancer statistics, 2024. *CA Cancer J Clin*. 2024;74(2):203. doi:10.3322/caac.21820
2. Tas F. Metastatic behavior in melanoma: timing, pattern, survival, and influencing factors. *J Oncol*. 2012;2012:647684. doi:10.1155/2012/647684

3. Koyama S, Akbay EA, Li YY, et al. Adaptive resistance to therapeutic PD-1 blockade is associated with upregulation of alternative immune checkpoints. *Nat Commun*. 2016;7(1):10501. doi:10.1038/ncomms10501
4. Shi H, Moriceau G, Kong X, et al. Melanoma whole-exome sequencing identifies (V600E)B-RAF amplification-mediated acquired B-RAF inhibitor resistance. *Nat Commun*. 2012;3(1):724. doi:10.1038/ncomms1727
5. Chapman PB, Hauschild A, Robert C, et al. Improved survival with vemurafenib in melanoma with BRAF V600E mutation. *N Engl J Med*. 2011;364(26):2507–2516. doi:10.1056/NEJMoa1103782
6. Hamid O, Robert C, Daud A, et al. Safety and tumor responses with lambrolizumab (anti-PD-1) in melanoma [published correction appears in. *N Engl J Med*. 2018;379(22):2185.
7. Villanueva J, Vultur A, Lee JT, et al. Acquired resistance to BRAF inhibitors mediated by a RAF kinase switch in melanoma can be overcome by cotargeting MEK and IGF-1R/PI3K. *Cancer Cell*. 2010;18(6):683–695. doi:10.1016/j.ccr.2010.11.023
8. Ugurel S, Paschen A, Becker JC. Dacarbazine in melanoma: from a chemotherapeutic drug to an immunomodulating agent. *J Invest Dermatol*. 2013;133(2):289–292. doi:10.1038/jid.2012.341
9. Demetri GD, Schöffski P, Grignani G, et al. Activity of eribulin in patients with advanced liposarcoma demonstrated in a subgroup analysis from a randomized Phase III study of eribulin versus dacarbazine [published correction appears in. *J Clin Oncol*. 2018;36(4):432.
10. Tagne JB, Kakumanu S, Nicolosi RJ. Nanoemulsion preparations of the anticancer drug dacarbazine significantly increase its efficacy in a xenograft mouse melanoma model. *Mol Pharm*. 2008;5(6):1055–1063. doi:10.1021/mp8000556
11. Davis ME, Zuckerman JE, Choi CH, et al. Evidence of RNAi in humans from systemically administered siRNA via targeted nanoparticles. *Nature*. 2010;464(7291):1067–1070. doi:10.1038/nature08956
12. Tatiparti K, Sau S, Kashaw SK, Iyer AK. siRNA delivery strategies: a comprehensive review of recent developments. *Nanomaterials*. 2017;7(4):77. doi:10.3390/nano7040077
13. Bartel DP. MicroRNAs: genomics, biogenesis, mechanism, and function. *Cell*. 2004;116(2):281–297. doi:10.1016/S0092-8674(04)00045-5
14. Fabian MR, Sonenberg N, Filipowicz W. Regulation of mRNA translation and stability by microRNAs. *Annu Rev Biochem*. 2010;79(1):351–379. doi:10.1146/annurev-biochem-060308-103103
15. Lee RC, Feinbaum RL, Ambros V. The C. elegans heterochronic gene lin-4 encodes small RNAs with antisense complementarity to lin-14. *Cell*. 1993;75(5):843–854. doi:10.1016/0092-8674(93)90529-Y
16. Simmons JL, Pierce CJ, Al-Ejeh F, Boyle GM. MITF and BRN2 contribute to metastatic growth after dissemination of melanoma. *Sci Rep*. 2017;7(1):10909. doi:10.1038/s41598-017-11366-y
17. Prykhozhij SV, Ban K, Brown ZL, et al. miR-34a is a tumor suppressor in zebrafish and its expression levels impact metabolism, hematopoiesis and DNA damage. *PLoS Genet*. 2024;20(5):e1011290. doi:10.1371/journal.pgen.1011290
18. Welponer H, Tsibulak I, Wieser V, et al. The miR-34 family and its clinical significance in ovarian cancer. *J Cancer*. 2020;11(6):1446–1456. doi:10.7150/jca.33831
19. Weeraratne SD, Amani V, Neiss A, Teider N, Scott DK, Pomeroy SL. Cho YJ: miR-34a confers chemosensitivity through modulation of MAGE-A and p53 in medulloblastoma. *Neuro Oncol*. 2011;13(2):165–175. doi:10.1093/neuonc/noq179
20. Xu Y, Guo B, Liu X, Tao K. Tao K: miR-34a inhibits melanoma growth by targeting ZEB1. *Aging*. 2021;13(11):15538–15547. doi:10.18632/aging.203114
21. Liu R, Xie H, Luo C, et al. Identification of FLOT2 as a novel target for microRNA-34a in melanoma. *J Cancer Res Clin Oncol*. 2015;141(6):993–1006. doi:10.1007/s00432-014-1874-1
22. Yamazaki H, Chijiwa T, Inoue Y, et al. Overexpression of the miR-34 family suppresses invasive growth of malignant melanoma with the wild-type p53 gene. *Exp Ther Med*. 2012;3(5):793–796. doi:10.3892/etm.2012.497
23. Pecot CV, Calin GA, Coleman RL, Lopez-Berestein G, Sood AK. RNA interference in the clinic: challenges and future directions. *Nat Rev Cancer*. 2011;11(1):59–67. doi:10.1038/nrc2966
24. von Karstedt S, Montinaro A, Walczak H. Exploring the TRAILs less travelled: TRAIL in cancer biology and therapy. *Nat Rev Cancer*. 2017;17(6):352–366. doi:10.1038/nrc.2017.28
25. Li B, Russell SJ, Compaan DM, et al. Activation of the proapoptotic death receptor DR5 by oligomeric peptide and antibody agonists. *J mol Biol*. 2006;361(3):522–536. doi:10.1016/j.jmb.2006.06.042
26. Vrielink J, Heins MS, Setroikromo R, et al. Synthetic constrained peptide selectively binds and antagonizes death receptor 5. *FEBS J*. 2010;277(7):1653–1665. doi:10.1111/j.1742-4658.2010.07590.x
27. Hu Y, Xu BH, Ji QX, et al. A mannosylated cell-penetrating peptide-graft-polyethylenimine as a gene delivery vector. *Biomaterials*. 2014;35(13):4236–4246. doi:10.1016/j.biomaterials.2014.01.065
28. Santos-Cuevas CL, Ferro-Flores G, Arteaga de Murphy C, et al. Design, preparation, in vitro and in vivo evaluation of 99mTc-N2S2-Tat(49-57)-bombesin: a target-specific hybridradiopharmaceutical. *Int J Pharm*. 2009;375(1–2):75–83. doi:10.1016/j.ijpharm.2009.04.018
29. Wu Z, Zhan S, Fan W, et al. Peptide-mediated tumor targeting by a degradable nano gene delivery vector based on pluronic-modified polyethylenimine. *Nanoscale Res Lett*. 2016;11(1):122. doi:10.1186/s11671-016-1337-5
30. Deshmukh AS, Chauhan PN, Noolvi MN, et al. Polymeric micelles: basic research to clinical practice. *Int. J Pharm*. 2017;532(1):249–268.
31. Leng Q, Goldgeier L, Zhu J, Cambell P, Ambulos N, Mixson AJ. Histidine-lysine peptides as carriers of nucleic acids. *Drug News Perspect*. 2007;20(2):77–86.
32. Nam K, Nam HY, Kim PH, Kim SW. Paclitaxel-conjugated PEG and arginine-grafted bioreducible poly (disulfide amine) micelles for co-delivery of drug and gene. *Biomaterials*. 2012;33(32):8122–8130. doi:10.1016/j.biomaterials.2012.07.031
33. Zhu S, Wonganan P, Lansakara-P DS, O'Mary HL, Li Y, Cui Z. The effect of the acid-sensitivity of 4-(N)-stearoyl gemcitabine-loaded micelles on drug resistance caused by RRM1 overexpression. *Biomaterials*. 2013;34(9):2327–2339. doi:10.1016/j.biomaterials.2012.11.053
34. Kumari S, Chauhan S, Umar A, Fouad H, Akhtar MS. Conductometric and fluorescence probe analysis to investigate the interaction between bioactive peptide and bile salts: a micellar state study. *Molecules*. 2022;27(21):7561. doi:10.3390/molecules27217561
35. Shinde VR, Revi N, Murugappan S, Singh SP, Rengan AK. Enhanced permeability and retention effect: a key facilitator for solid tumor targeting by nanoparticles. *Photodiagnosis Photodyn Ther*. 2022;39:102915. doi:10.1016/j.pdpdt.2022.102915
36. Fröhlich E. The role of surface charge in cellular uptake and cytotoxicity of medical nanoparticles. *Int J Nanomed*. 2012;7:5577–5591. doi:10.2147/IJN.S36111